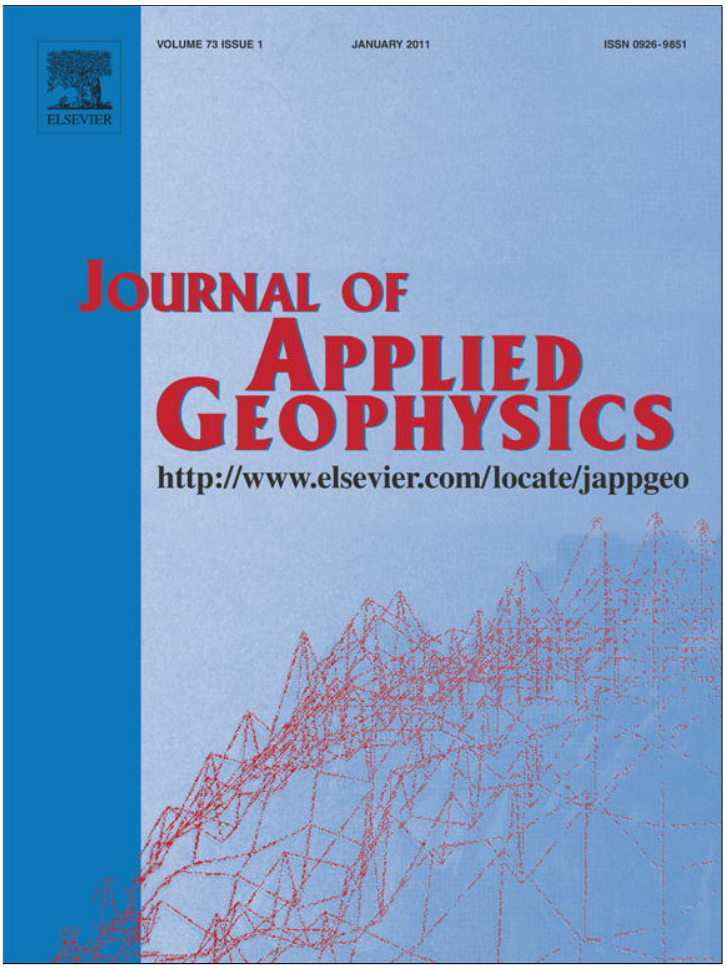

(This is a sample cover image for this issue. The actual cover is not yet available at this time.)

Journal of Applied Geophysics 75 (2011) 603–614

Contents lists available at SciVerse ScienceDirect

Journal of Applied Geophysics

journal homepage: www.elsevier.com/locate/jappgeo

Optimal filtering high-resolution seismic reflection data using a weighted-mode empirical mode decomposition operator

Leonardo Macelloni [a,*], Bradley Matthew Battista [b], Camelia Cristina Knapp [c]

[a] Mississippi Mineral Resources Institute, Center for Marine Resources and Environmental Technology and the Seabed Technology Research Center, University of Mississippi, 111 Brevard Hall, University, MS 38677, USA
[b] EnerGeo Solutions 804 Mohawk Drive West Columbia, SC 29208, USA
[c] Department of Earth and Ocean Sciences, University of South Carolina, 701 Sumter St. Columbia, SC, USA

ARTICLE INFO

Article history:
Received 14 February 2011
Accepted 18 September 2011
Available online 25 September 2011

Keywords:
High resolution seismic
Optimal filtering
EMD
Time-domain digital processing
Gas hydrates
Gulf of Mexico

ABSTRACT

Gas-hydrate related processes in deep-water marine settings exist on spatial scales that challenge conventional seismic reflection profiling to successfully image them. The conventional approach to acoustic identification of buried hydrates is to use advanced, cost-prohibitive survey techniques and highly customized software to define subsurface structure wherein compositional changes may be modeled and/or interpreted. This study adopts a different approach derived from recent theoretical advancements in signal processing. The method consists in optimal filtering high resolution, single-channel seismic reflection data using the Empirical Mode Decomposition (EMD). The time series is decomposed in sub-components and the noisy portions are suppressed adopting the technique that we referred as Weighted Mode(s) EMD. The optimal filtering greatly improves the resolution and fidelity of the seismic data set.
High Resolution single channel seismic profiles, acquired over a carbonate\hydrates site in the northern Gulf of Mexico, manipulated in such way, show a complex, shallow subsurface, and suggest potential evidence for buried gas hydrates.

1. Introduction

The Gulf of Mexico Hydrates Research Consortium (GOMHRC) was established in 1999 as a joint venture between USA Academia, Industry, and Federal entities with a focus on consolidating and improving basic and technical research of gas hydrates in the Gulf of Mexico. The main goal of the Consortium is to install and operate the first permanent sea-floor monitoring station which will monitor more or less continuously the Gas Hydrates Stability Zone (GHSZ) via geochemistry, geophysical and biological measurements (McGee, 2006). In order to facilitate the best observatory site selection, over the last few years the GOMHRC has been carrying out several seismo-acoustic surveys around the Northern Gulf of Mexico continental Shelf using the Surface Source Deep Receiver (SSDR) technique (McGee, 2000). This custom-developed seismic device could provide with a reasonable low cost very good seismic images of up to 500–700 m of sediments, with a vertical resolution of <1 m (Macelloni, 2005). In order to fully exploit the potential of this system, it has been demonstrated by McGee (1997, 2000) that acquisition must exercise particular care to preserve a very broad band and a high fidelity signal. This is accomplished by digitizing the signal as fast as possible (up to 100 kHz) and using a high dynamic range (24 bit). At the same time digital signal processing must preserve such characteristics by avoiding any possible signal distortion or loss of information carried by the signal. Time-domain signal processing is a very suitable tool for this application, especially for signals that show non-stationary behavior. Recently several new techniques have been developed and tested, and good success has been obtained by the adoption of Empirical Mode Decomposition (EMD). Despite a quite large use of this technique in several fields of digital signal processing (Pai et al., 2007; Schmitt et al., 2007; Sweeney-Reed and Nasuto, 2007) only a few examples have been shown in geophysical data processing (Addison et al., 2009; Battista et al., 2007, 2009; Magrin-chagnolleau and Baraniuk, 1999).

The objective of this paper is to present a new technique in optimal filtering high resulting seismic data using the Weighted-Mode EMD. In fact, time-domain digital processing using EMD allows a signal to be separated into several independent subcomponents. The portion of the signal spectrum judged to be noise or lacking in geological information is subsequently suppressed by scaling down the amplitudes of those subcomponents using the Weighted Modes filter bank. The final result is a highly detailed seismic image of the subsurface, which confirm how valuable information from gas hydrates occurrence and distribution, can be obtained combining non-standard high resolution seismic data collection and non-conventional time-domain digital signal processing.

* Corresponding author at: Mississippi Mineral Resources Institute. 111 Brevard Hall, University, MS 38677-1848, USA. Tel.: +1 6629157320; fax +1 6629155625.
E-mail address: lmacello@olemiss.edu (L. Macelloni).

0926-9851/$ – see front matter © 2011 Elsevier B.V. All rights reserved.
doi:10.1016/j.jappgeo.2011.09.018

2. Imaging a complex shallow subsurface geological system in deep water

Mississippi Canyon Block 118 Mound (MC118, Fig. 1) represents a mature example a complex carbonate\hydrate with a fault migration-conduit system overlying shallow salt directly connected to deeply-buried source rocks for gas and oil (Knapp et al., 2010; Sassen et al., 2006). Several submersible missions to the seafloor have identified large gas hydrate outcrops, authigenic carbonate mounds, several bubble and oil vents, and chemosynthetic communities (Macelloni et al., 2010; Sassen et al., 2006). The south-central portion of MC118, in roughly 900 m of water, overlies Pliocene-to-Pleistocene salt that is facilitating hydrocarbon venting in response to more recent (perhaps Holocene) mass slumping events resulting from slope instability. The mound is characterized by three principle venting and/or paleoventing clusters as reported by Sleeper et al. (2006) and Macelloni et al. (2010). Lapham et al. (2008) give the geochemical interpretation of the seabed in response to the underlying hydrocarbon sources while Knapp et al. (2010) detail the underlying structures and pathways for hydrocarbon migration.

The shallow subsurface structures in MC118 are typical of salt-intrusion structures but are also a challenge for remote sensing. Hydrocarbon-related structural complexity manifested as high-order faulting and brine and gas migration have been noted by Wood et al.(2002), Lutken et al. (2003), and Hardage and Roberts (2006). Hardage and Roberts (2006) review the targets of seismo-acoustic instrumentation for such kind of scenario in the Gulf of Mexico. They argue that successful acoustic imaging of hydrate related processes with seismic reflection method is highly dependent on the spatial and temporal sampling resolution of the data and the ability to preserve phase and amplitude of weak signals during processing.

3. Data and method

The surface source, deep receiver (SSDR) is a seismic profiling method developed to provide high-resolution images of shallow sub-bottom features in deep water. The SSDR recording geometry is shown in Fig. 2. If the receiver is deployed far enough below the source, the direct wave from source to receiver can be considered to be the source's far-field signature (Ziolkowski et al., 1982; Ziolkwoski, 1987). If the receiver is high enough above the sea floor, the direct wave can be recorded without interference by other seismic waves such as the sea-floor reflection. When both conditions are fulfilled, digital processing can “collapse” the direct waveform and the waveforms of sub-bottom reflections. This establishes reflection polarity and substantially increases the resolution with which sub-bottom structure can be imaged. The “collapsed” waveforms can then be scaled so that their amplitudes can be used to estimate physical properties across the reflecting interfaces.

A grid of SSDR profiles was acquired over the mound portion of MC118 (Fig. 3). Nominal spacing is 50 m between north–south

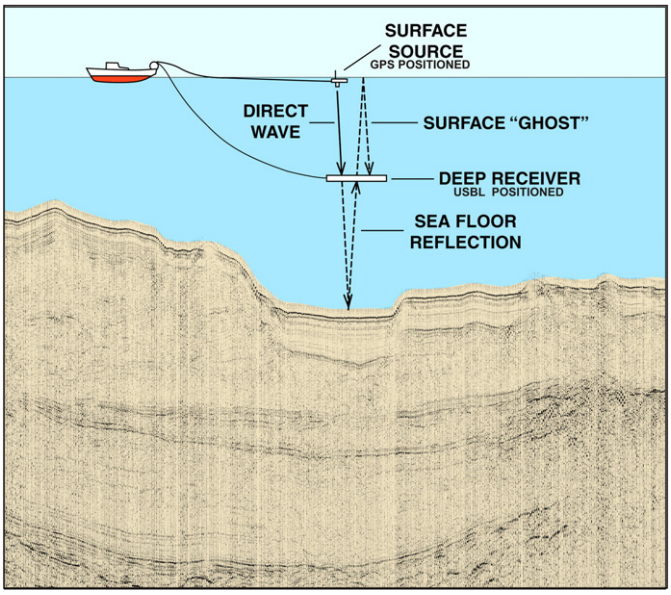

Fig. 2. SSDR survey geometry cartoon. Schematic of the seismic reflection acquisition geometry. This geometry significantly separates ghosts and multiples from the shallow sediments of interest.

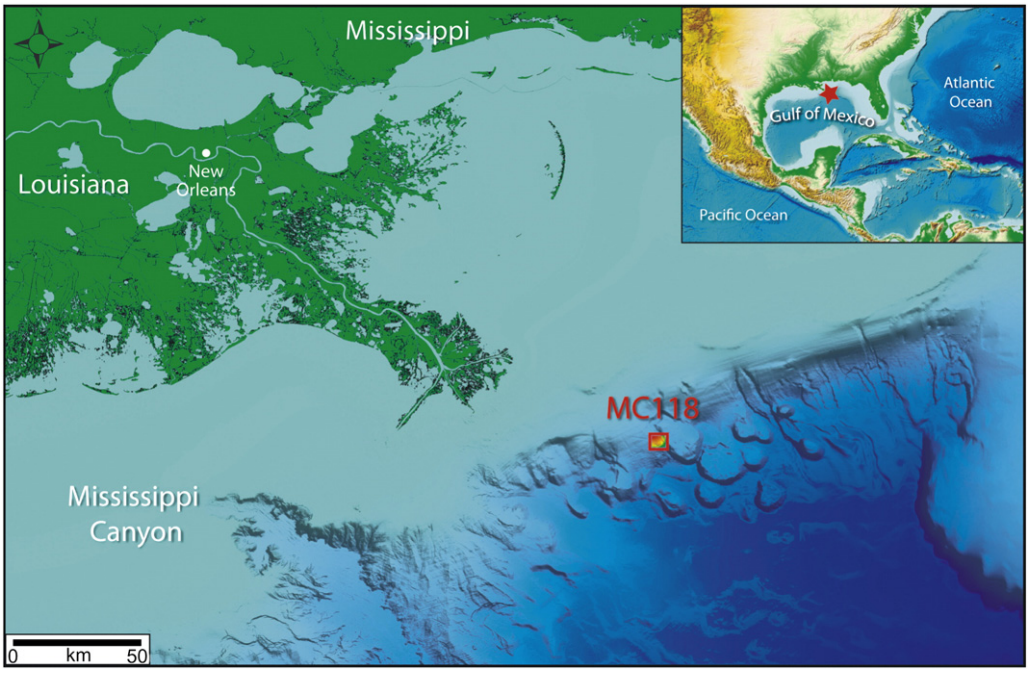

Fig. 1. Area of study. Location map for Mississippi canyon block 118 (MC118).

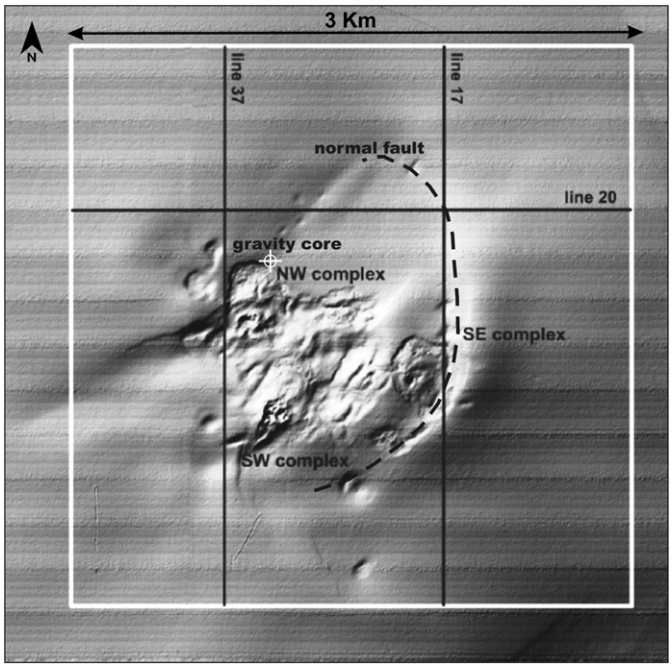

Fig. 3. Map of seismic lines position. Basemap showing processed seismic reflection lines and venting complexes overlying bathymetry in MC118. The white site box is about 3×3 km and depicts the area where the seismic grid has been acquired. The dot line indicates the planar position of a large normal fault mapped over the seismic grid, while the white circle indicates the position where a gravity core, recovered solid gas hydrates inclusions.

profiles and 100 m between east–west profiles. A total of 96 profiles with a trace to trace distance of ≈10 m were recorded. The whole survey comprises about 30,000 traces. A 80 cubic inch Sodera water-gun was selected as the seismic source because it provides both a broad bandwidth and sufficient power to penetrate the hydrate stability zone. The source was independently positioned via a differential GPS system. A single-channel hydrophone receiver was towed 350–400 m deep beneath the source. The receiver location was real-time tracked using a 200 kHz Linquest Ultra Short Base Line (USBL) system. The data were digitally recorded using a digital recording system, custom built by Lookout Geophysical, at 100 KHz and 24 bit. McGee (2000) reviews the benefits of this high simple rate ("oversampling") of the seismic signals. The main improvements are smoother antialiasing of the analog-to-digital conversion, phase preservation, and increased temporal [depth] resolution. Most importantly, oversampled digital signals better represent their analog parents which allows for accurate geologic information of increased bandwidth and resolution to be extracted from them. Recording at 100 KHz with the SSDR allows for the aforementioned benefits but not without cost. Fig. 4 shows low-frequency strumming of the receiver cable and high-frequency interference from the acoustic positioning equipment. Both are strong, disruptive noise significantly masking geologic information. Optimally attenuating this noise is critical to preserving and imaging the geologic information.

4. Method: adaptive, nonlinear processing flow

Seismic reflection data from MC118 have two primary sources of acquisition noise and one type of noise that is a geologic response. Both of the acquisition system noise sources, receiver cable strum and USBL interference, differ in nature. Cable strum is a high-amplitude, nonlinear process of tow-cable strumming in the water column, and it is limited to low frequency. Interference from the USBL is patterned in time according to the ratio of its sampling frequency to that of the seismic imaging source. It is strongest at frequencies higher than our expected geologic information but lower than our sampling frequency. Both cable strum and USBL noise can be seen together in the "suppressed" trace in Fig. 5. The "geologic" noise is not apparent here but is addressed later in the text. This work demonstrates how optimum results are produced by manipulating the results of the empirical mode decomposition (EMD). The results are very clean seismic data with all of the attributes for geologic information left intact for additional processing and interpretation.

The empirical mode decomposition was first introduced by Huang et al. (1998) and adapted for work with seismic reflection data by Magrinchagnolleau and Baraniuk (1999) and Battista et al. (2007). The principle of this technique is to decompose a signal $c(t)$ into a sum of functions that:

(1) have the same numbers of zero crossings and extrema;
(2) are symmetric with respect to the local mean.

The first condition is similar to the narrow-band requirement for a stationary Gaussian process. The second condition modifies a global requirement to a local one, and is necessary to ensure that the instantaneous frequency will not have unwanted fluctuations as induced by asymmetric waveforms. These functions are called intrinsic mode functions (IMFs), and denoted $imf_i(t)$. The intrinsic mode functions are obtained using the algorithm illustrated in the scheme below

1) Initialize: $r_0(t) = x(t)$, $i = 1$
2) Extract the i-th IMF:
   a. Initialize: $h_0(t) = r_i(t)$, $j = 1$
   b. Extract the local minima and maxima of $h_{j-1}(t)$

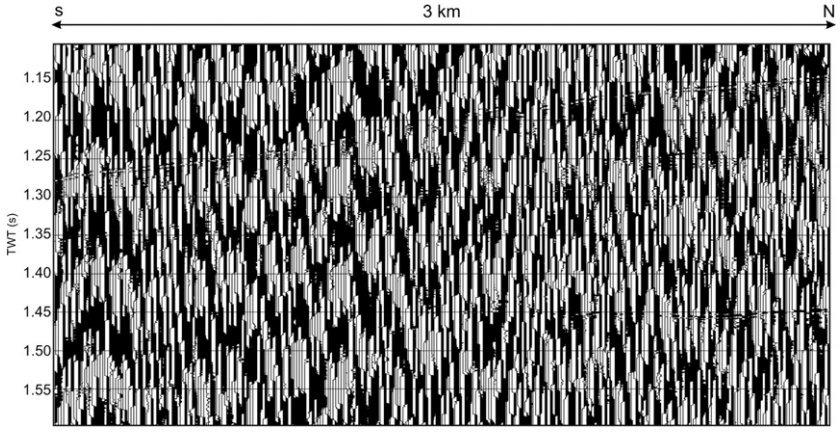

Fig. 4. Example of raw seismic data. Raw data exhibiting strong cable strum noise resulting as the deep receiver is towed through the water column. Overprinting this cables strum noise is high frequency, horizontal bands caused by receiver positioning instruments in our oversampling frequencies (>3 kHz). The seafloor and subsurface are seen as the weak horizons dipping from left to right.

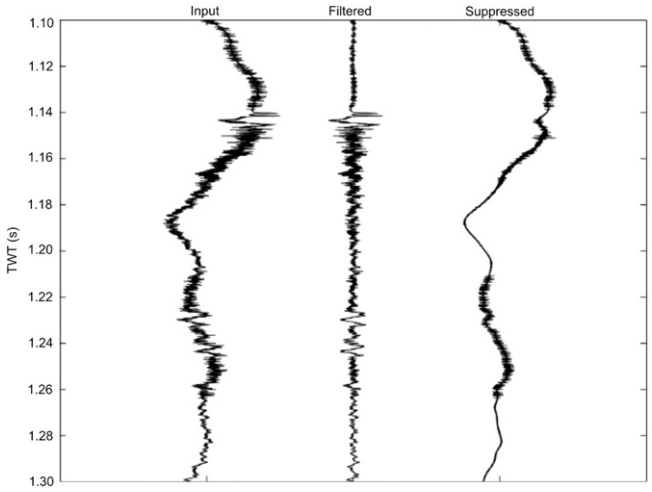

Fig. 5. Optimal filtering using partial EMD. The input trace on the left is filtered to produce the middle trace. The trace on the right shows information suppressed. It contains the two dominant types of noise evident as strong, low frequency cable strum with high frequency USBL interference. It is important to note that the residual noise on the right is scaled to low amplitude, not removed.

c. Interpolate the local maxima and the local minima by a cubic spline to form upper and lover envelopes of $h_{j-1}(t)$
d. Calculate the mean $m_{j-1}(t)$ of the upper and lover envelopes
e. $h_j(t) = h_{j-1}(t) - m_{j-1}(t)$
f. if stopping criteria is satisfied then set $imf_i(t) = h_j(t)$; else go to b with $j = j + 1$

3) $r_i(t) = r_{i-1}(t) - imf_i(t)$
4) if $r_i(t)$ still has at least 2 extrema then go to 2 with $i = i + 1$ else the decomposition is finished and $r_i(t)$ is the residue.

At the end of the algorithm, we have:

$$c(t) = \sum_{i=1}^{n} imf_i(t) + r_n(t). \quad (1)$$

Where $r_n(t)$ is the residue of the decomposition. Each of the components is produced by removing "mean splines" from the data by a process referred to as sifting. Fig. 6 illustrates a mean spline. It is produced by first locating the extrema, or peaks and troughs, of a signal. Two cubic-spline curve fits are determined as the envelope of the signal. The average of this envelope is the mean spline, and it is successively determined and subtracted until it is locally zero anywhere in the time series.

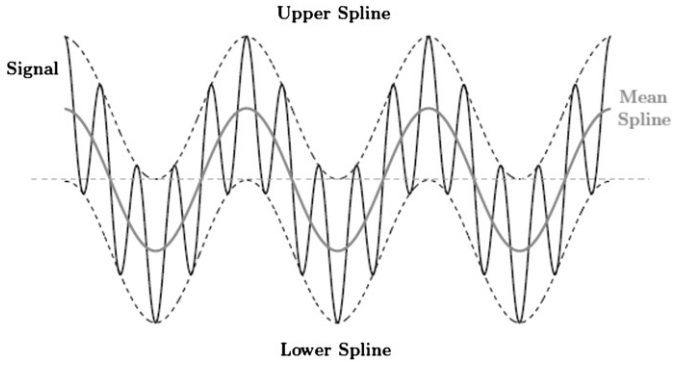

Fig. 6. The mean spline. Mean spline produced as the mean of the upper and lower cubic spline fits to a time series.

The objective of sifting a time series is to produce the IMFs. Intrinsic mode functions are defined as having zero mean, equal number of zero crossings and extrema, and that the number of peaks and troughs be equal or differ by no more than one. Further, the first IMF produced contains the highest frequency content of the time series since all of the low-order components causing a non-zero mean have been empirically removed. Therefore, repetitively removing IMFs and sifting the result effectively decomposes the time series into its lowest order components until there are no more definable components The EMD is a data-driven process that is well suited for handling data from both stochastic and astochastic processes. It works by sifting out trends to produce modes, and then by removing modes until the result is the lowest order representation of the original signal. The result of EMD is to produce a set of locally stationary oscillations, the sum of which yields the original time series. More specific to this work; however, is that the set of sub-functions undergoes some change before taking the sum and that signal attributes be preserved while doing so. Proper application of EMD produces a series of IMFs possessing ideal characteristics for traditional processing. The reason is given by their criteria— the aforementioned zero mean, zero crossings, and extrema conditions.

Seismic pulses, in theory, possess these characteristics but are also causal (time limited) which suggests that the conditions for an IMF may never be completely met without first modifying the signal. Intrinsic mode functions derived from seismic pulses are best handled in the time domain for this reason.

4.1. Detrending with EMD

Normal EMD allows trends to be sifted from each mode until that mode becomes an IMF. Thus, EMD is allowed to define information "intrinsic" to the signal, and isolation or combination of select modes allows those characteristics to be enhanced before summing the modes. However, IMFs in some cases may not be able to characterize signal and noise in such a way to allow them to be completely separated. This problem occurs when multiple events with the same time-varying characteristics are present. Seismic reflection multiples, for example, cannot be separated using EMD. However, events having different time-varying characteristics are highly separable by EMD. Further, using the EMD to produce trends that are not IMFs expands its use as a detrending tool as first observed by Wu et al. (2007).

This possibly stems from the conditions that

1) forcing the EMD to sift too far produces more or less pure tones that may or may not be intrinsic to the signal and
2) forcing the EMD to stop sifting too early produces a trend that is intrinsic to the signal but may not satisfy the criteria for an IMF.

Either approach can be used to expand the types of signals produced by the EMD; however, the results may be trends that are not IMFs. Special attention to governing the integrity of IMFs is addressed by Wu and Huang (2004) and Rilling et al. (2004). However, "partial" EMD, or EMD without a strict focus on producing IMFs, may be used to improve computational efficiency while still outperforming conventional detrending utilities.

Seismic reflection data from MC118 are decomposed into twelve modes per trace using the partial EMD approach. The objective of partial EMD is to focus computational effort where signal and noise require careful separation while passing the remaining information into separate modes. Four partial and one complete EMD are performed on each trace. Each partial mode consists of one mode and one residual. Each residual is taken as the input for its following EMD. The last residual is allowed to be completely decomposed, and all of the modes from all five EMDs are retained in a mode bank. The first three partial EMDs are limited to only three sifts. This technique effectively produces the first three modes of the bank, and they are characterized as having all frequencies including and above

those which contain USBL interference. The remaining residual contains the desired geologic information and the low-frequency cable strum. The fourth EMD is limited to two sifts such that most of the geologic signal is passed into its output mode; it resembles the result of a conventional bandpass operator because the effective bandwidth of the geologic information is present. The fifth EMD is designed to separate any remaining signal from cable strum, and it effectively does this with five modes of twenty sifts each.

Determining how many EMDs to apply and how many times to sift for each mode of each EMD is done manually by analyzing random traces until the limits of geologic information are reduced to only a few modes in the center of the mode bank. Fig. 7 illustrates the procedure. The benefit of this technique is that the EMD's computational demand is reduced by over 100 times as determined by the length of time required to produce the mode bank. The advantage of this technique is that any well-defined time-varying characteristic intrinsic to the signal may be isolated for further processing.

4.2. Weighted-mode EMD

Typical usage for EMD is to decompose a signal to several modes which can be processed in any number of ways. Using the EMD as a detrending tool requires that some or all of the modes be summed to form the filtered output considering that the sum of unprocessed modes reproduces the original signal. In theory, modes produced by partial EMD are not true IMFs and must not be excluded from the mode bank before calculating the sum; but we have seen that partial EMD is much more efficient in term both of computational speed and operator versatility. Therefore we introduced the weighted mode EMD, in which partial IMF are not simply removed from the mode bank, but instead, weighted [modulated] to lower amplitude. The goal of weighting modes produced by (partial) EMD is to produce a summed output trace containing significantly more geologic information than it does noise. The process of doing so requires a bank of modes adequately separating targeted trends such as geologic information from undesirable trends. Fig. 5 illustrates a typical trace from the SSDR system and sample results for suppressing noise. The modes produced by the partial EMD are found in Fig. 7. Modes containing both signal and noise suggest

1) a poorly defined partial EMD and
2) that there is an optimum "resolution" of EMDs and sifts for decomposing a given seismic trace.

Fortunately, survey, hardware, and environmental conditions generally remain constant during seismic reflection data acquisition. Therefore, the assumption may be loosely held that a partial EMD designed for a few traces is applicable to a larger data set, and the data used herein are an excellent case in point. Nearly all of the partial EMDs produce the results shown in Fig. 7 where the geologic information is found between the second and seventh modes. A mode-picking strategy and a weighting function are all that remain once a partial EMD is designed.

Selection of weights for the bank of modes from (partial) EMD provides the greatest advantage for using EMD as a time-domain processing utility. The number of modes in the bank, together with the weighting scheme, gives tremendous control over the information therein. The actual weighting function is a list of scaling factors to multiply by each mode in the bank before summing to produce the output trace. To start, the target modes to keep are chosen. A cumulative summation of increasing and decreasing mode order is used to select the target modes because it is sometimes difficult to identify signal from a signal mode. Fig. 8 shows how the cumulative sum analysis compares to the input trace.

This technique is very useful and powerful for bounding the input signal within a range of modes. The cumulative sum analysis provides

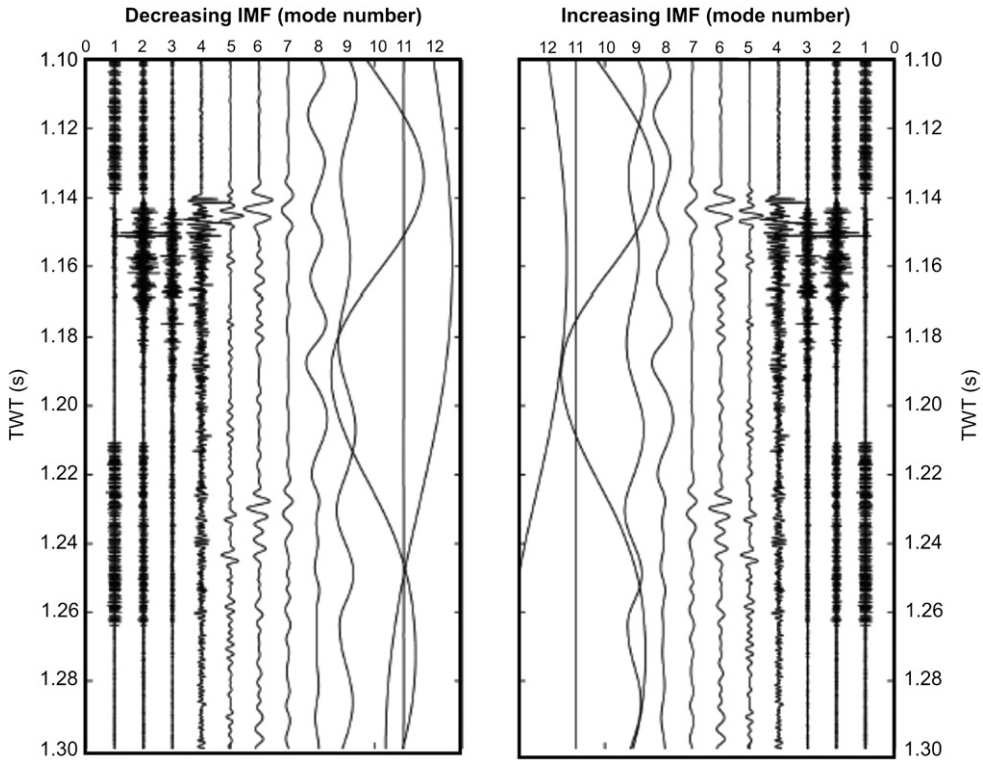

Fig. 7. Partial EMD on seismic reflection traces. Panels showing modes produced by partial EMD. The modes are sorted by decreasing frequency in the left panel and by increasing frequency in the right panel. Mode one contains the USBL interference, two through seven contain geologic information, and eight through twelve are all related to cable strum. Amplitude has not been modified. The high amplitude noise of low frequency is related to receiver cable strum. A cumulative summation of the traces in each panel provides a nice tool for windowing signal within these modes.

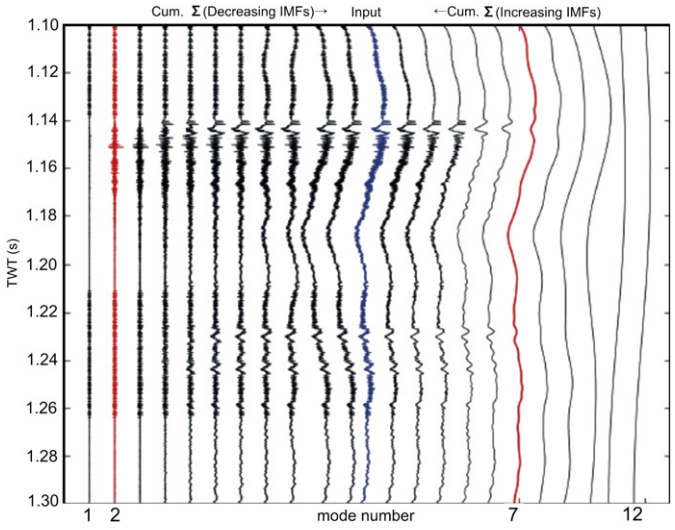

Fig. 8. Partial EMD mode(s) sum panel of a seismic trace. Cumulative sums of the panels in Fig. 7. Traces left of the input (blue) are cumulative sums of high-frequency modes whereas traces to the right are cumulative sums of low-frequency modes. All modes contributing signal to the cumulative sum fall between the red traces. Note that the x-axis resets at the input trace. (For interpretation of the references to color in this figure legend, the reader is referred to the web version of this article.)

only the mode numbers in the mode bank where targeted information resides. The weighting scheme chosen here is to leave modes containing geologic information unscaled except for the bounding modes, and to apply a logarithmic function to the rest. Logarithmic functions are used because they handle signal power more effectively than do linear functions. The bounding modes are included with the scaling modes to provide a smooth transition between signal and noise. The bounding and outlying modes are weighted toward zero by powers of ten decided by that mode's distance from a bounding mode. For example, the bounding modes from Fig. 8 are two and seven. Modes lower than two and greater than seven are weighted by Eq. (2).

$$wt_n = \begin{bmatrix} 10^{-(lm-n+1)}, n \le lm \\ 10^{-(n-um+1)}, n \ge um \\ 1, lm < n < um \end{bmatrix} \quad (2)$$

where n is the mode number, lm is the lower bounding mode number, um is the upper bounding mode number, and wtn is the weighting factor. Given that there are twelve modes for every trace, example weights for bounding modes of two and seven would use 10^{-n}, where n = {2; 1; 0; 0; 0; 0; 1; 2; 3; 4; 5; 6}. These are referred to as the 2–7 weights. The 2–6 weights have bounding modes of two and six and use n = {2; 1; 0; 0; 0; 1; 2; 3; 4; 5; 6; 7}. Fig. 9 compares unscaled modes to weighted modes. The weighted modes are summed to give the results in Fig. 5. Most of the data processed use the 2–7 weights while a very small number of traces require the 2–6 weights. Both of these weighting series provide a similar result to a bandpass operator; although, no frequencies have been eliminated and the entire time-domain process uses data derived from the signal. In this manner, the signal undergoes band-modulation in the sense that portions of bandwidth are suppressed [modulated] in the time domain.

4.3. Signature processing

Water-gun data require extensive post processing because the duration of a water-gun signature is too long to provide good resolution and the waveform is not consistent from shot to shot. Processing the direct waves to remove their spectral phase improves both resolution and consistency (Macelloni, 2005). A water-gun generates a signal of nearly 100 ms duration. SSDR processing collapses the most of the energy into a peak of about 2 ms duration (Fig. 10). Thus the processing represents an improvement in resolution by a factor of about 50. Also,

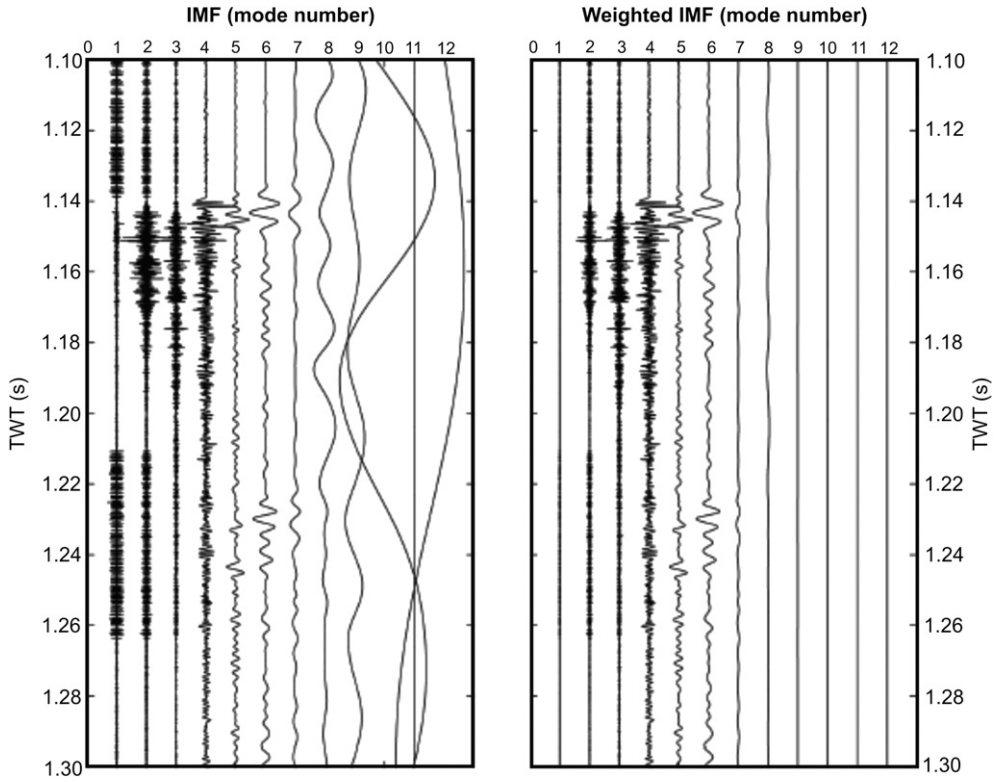

Fig. 9. Weighted-modes EMD filter bank. Panels comparing modes before (left) and after (right) being scaled by a logarithmic weighting function. Each mode in the left panel is multiplied by the scaling factor determined by Eq. (2) before summing to produce the filtered trace.

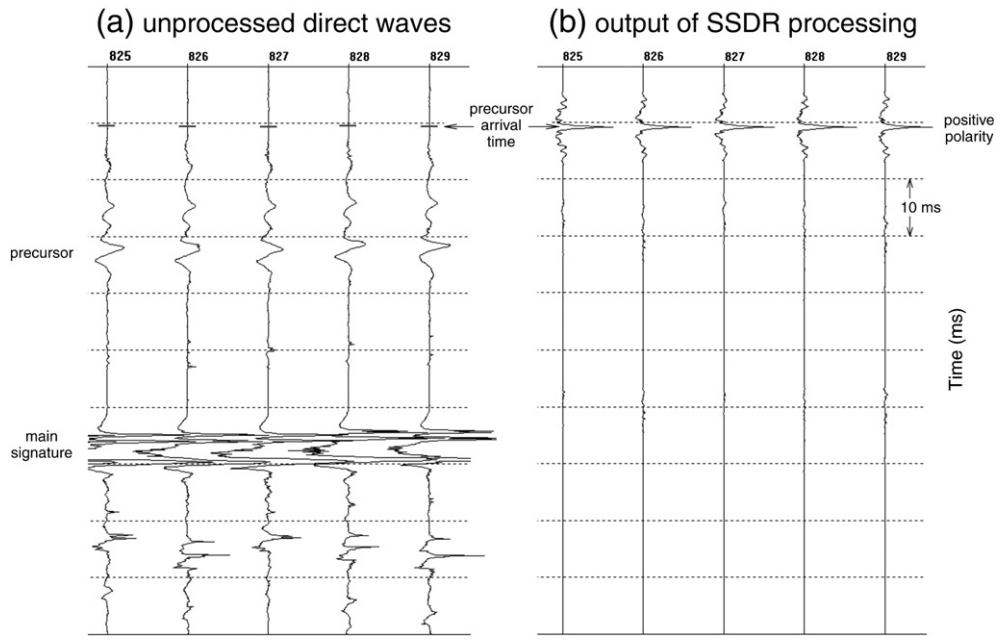

Fig. 10. Water gun signature processing. The raw water gun far field signature (a) is a broad and inconsistent seismic pulse; phase conjugation processing (b) collapses the pulse into a narrow signal increasing the vertical resolution.

the output is more consistent from shot to shot than is the input. Further the data were corrected for wave-front divergence and variations in energy level, for the static shift due to variation in the depth of the receiver and time migrated.

5. Results

A complete seismic reflection line from MC118, Line37ns, is processed using weighted-mode EMD. All of the parameters described above are employed. The raw data in Fig. 4 show very strong noise overprinting a weaker geologic signal indicated by dipping reflectors. As mentioned above, most of the noise is optimally removed using the twelve-mode, "2–7" weighting scheme. The strongest noise, receiver cable strum, must be addressed first. Cable strum is optimally suppressed by weighting all modes greater than mode seven. Mode seven is scaled by a factor of 10^{-1}, eight scales by 10^{-2}, nine scales by 10^{-3}, and so on. The filtered result in Fig. 11 shows that the receiver cable strum has been effectively suppressed. The high-frequency noise from the USBL interference is now quite apparent and is the second target for band modulation. The high-frequency USBL noise is just as easy to suppress as the cable strum noise and can even be done at the same time. Mode two is taken as the bounding mode for high frequency data. Mode two is scaled by a factor of 10^{-1} and mode one is scaled by 10^{-2}. The result in Fig. 12 is now a very high quality seismic reflection line having only localized noise. Localized noise is almost always addressed on a per trace basis because it may not have a well-defined source. However, the remaining vertically oriented bursts of energy seen above and below the seafloor horizon have been identified as electronic grounding problems on board the vessel. These noise bursts maintain a loose set of characteristics allowing them to be suppressed by shifting the low-frequency bounding mode from seven to six. Fig. 13 illustrates the line without this noise below the seafloor horizon.

6. Discussion

The practice of using nonlinear tools with seismic reflection data has forced integration of two historically distinct roles for geophysicists: the first being as a signal processor and the second being a geologic interpreter. Application of weighted-mode EMD in this work moved forward by characterizing noise in the time domain. This approach is quite effective given that most noise in seismic reflection

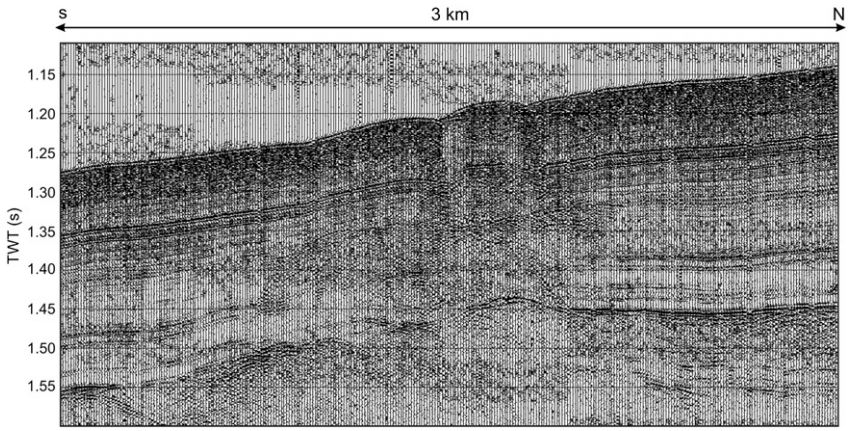

Fig. 11. Weighted-modes EMD, low-frequency noise reduction. Results of using EMD for suppressing strong, low-frequency noise caused by receiver cable strum. The remaining horizontal bands of darker shade are high frequency USBL noise. They are removed in Fig. 12.

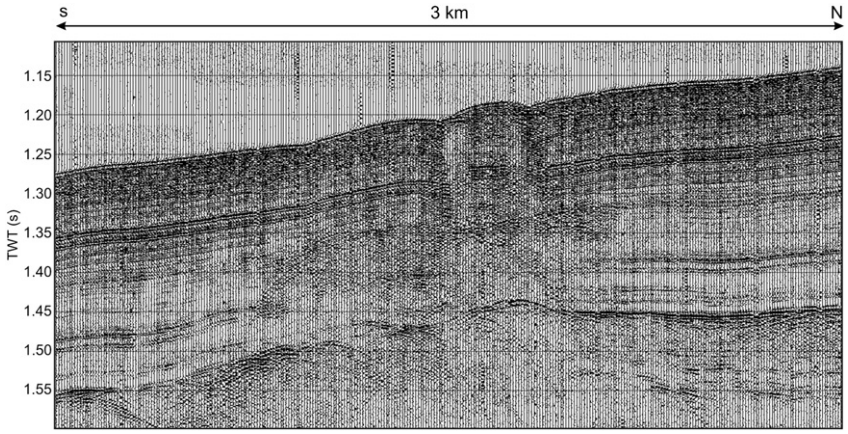

Fig. 12. Weighted-modes EMD, high-frequency noise reduction. High-frequency noise suppression. Noise caused by the ultra-short baseline used for subsurface positioning of the source and receiver is easily removed.

data is caused by either the environment or the equipment. The geologic information remains fixed while the survey is conducted. All of the traces processed produce a result resembling that of Fig. 5 where noise has been dampened, not removed, dramatically inverting the signal-to-noise ratio in favor of the geologic content of the signal. The following section reviews the geologic information to demonstrate how well the data have been processed.

Three lines from the data set in MC118 are chosen to demonstrate the interpretability of the results from using weighted-mode EMD. Fig. 3 shows the locations of these lines relative to the seafloor mound structure. All of the lines have had only this processing applied, and the processing scheme uses the 12-mode, "2–7" configuration followed by the "2–6" scheme for any additional noise. The scheme works well as all of the lines offer a great deal of information. Line37sn served as the example for processing and is the first to illustrate interpretability.

6.1. Line37ns

Line 37 ns runs alongside the northwestern and through the southwestern venting complexes shown in Fig. 3. It is the only line to show a deep-reaching venting system. Various amplitude fluctuations are seen below two seafloor pock marks. These features are clear in Fig. 14. Amplitude brightening may be suggestive of either changes in geology composition or fluids flux. Brightening occurs in two forms: the first one is the traditional high-amplitude, reversed polarity bright spots related to free gas which occurs in the deeper section (box 1, Fig. 14); the second as a new form, which is seen mostly near the seafloor but sometimes reaching deeper to the next significant stratigraphic unit (box 2, Fig. 14). This newer form of brightening is characterized by wavelengths on the order of microseconds and can only be imaged by phase preservation of oversampled data. The next unit underlying the brightened shallow sediments is characterized by several diffractions in the venting area. Acoustic wipeout, as highlighted in box 2, Fig. 14, is also quite common in this unit. Large part of the acoustic wipeout is manifested in chimney-like patterns indicative of pore fluid and/or gas migration upwards through the sediments. The chimneys like structure seem originate at the high-amplitude negative horizon which appears near 1.45 seconds in the north and dipping to 1.5 s in the south. This horizon, interpreted as free gas, could mark the base of the Hydrate Stability Zone (HSZ) and therefore assume the definition of "BSR". Theoretical model by Lapham (2008) using the MC 118 hydrates composition from Sassen et al. (2006) has placed the base of the stability zone at a comparable depth. The Lapham's model assumes the presence of a salt body at near surface, and, in fact, the top of a salt body has been identified in proprietary industry seismic data at about 1.7 s. therefore deeper than the data used in this work. Further, the seismic horizon marking the "BSR" appears discontinuous and segmented, as reported by Wood et al. (2008) for BSRs in Gulf of Mexico salt driven, hydrates system.

6.2. Line17ns

Situated north–south in the southeastern venting complex (Fig. 3) is Line17ns. This profile is perhaps the most dramatic line because, as shown in Fig. 15, it lies in an area having little to no seafloor expression of venting. However, the similarity between the southwestern

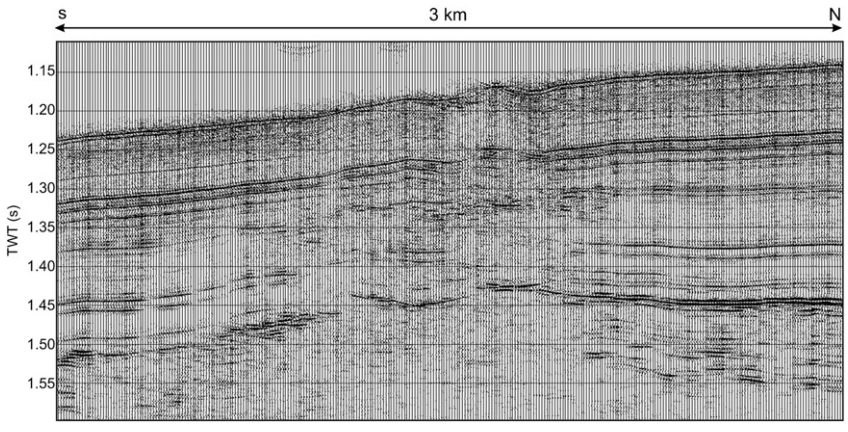

Fig. 13. Weighted-modes EMD intra-band noise reduction. Additional noise closer into the signal's peak bandwidth is suppressed by weighting particular IMFs before summation.

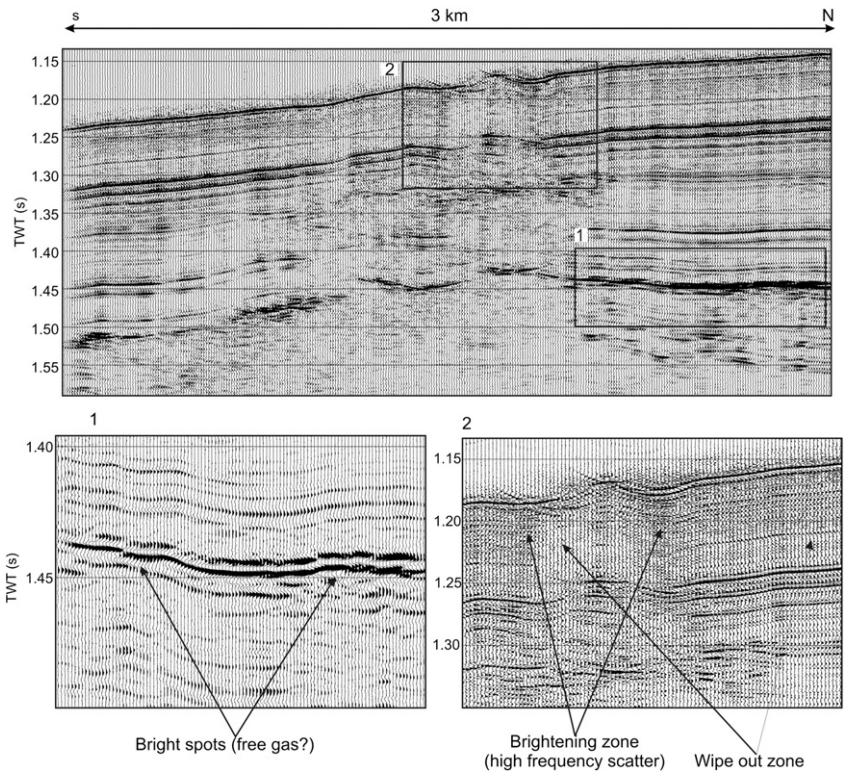

Fig. 14. Processed Line37ns. Line37ns runs north (right) to south (left) over a venting location having a seafloor extent. Free gas and/or pore fluids driven away from underlying salt are reaching the seafloor. Areas within the boxes show a possible reverse polarity bright spot (box 1), interpreted as free gas, and characteristic amplitude wipeout (box 2). Further, a new form of brightening areas are seen throughout the system (box 2).

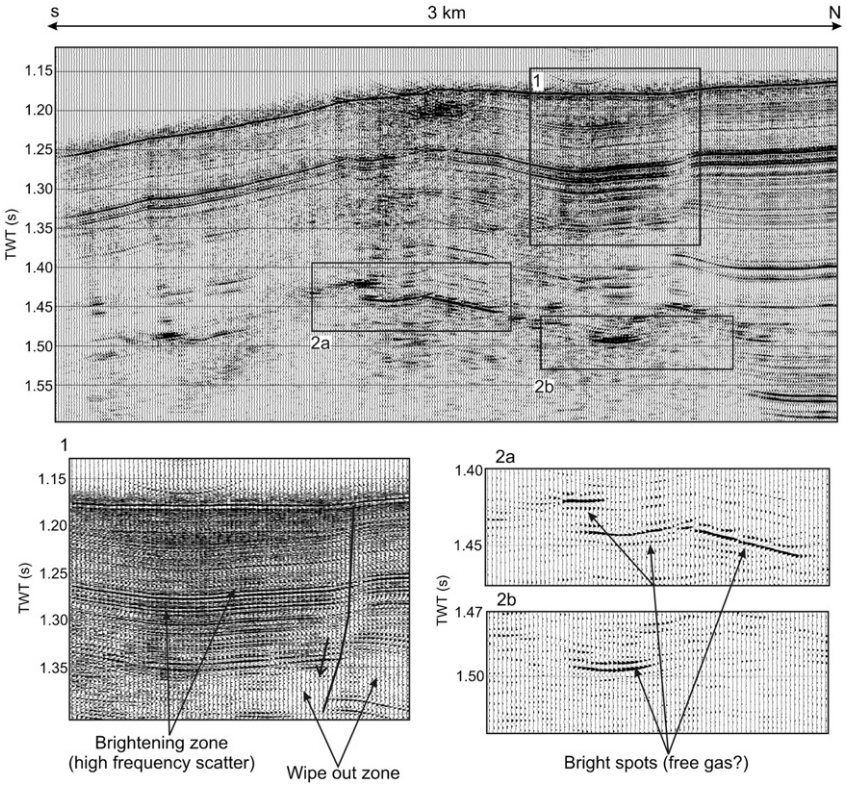

Fig. 15. Processed Line17ns. Line17ns runs north (right) to south (left). No observable seafloor venting is observed even though there appear to be several signs of migration pathways. A notable feature is the deep-reaching amplitude brightening associated with the filled basin in the shallow sediments (box 1). Reverse polarity bright spot is highlighted in box 2.

and southeastern venting complexes suggests activity, or at least past activity, here as well. Amplitude brightening is again shown but is mostly associated with a now filled fault-controlled basin (box 1 Fig. 15). The fault has a parabolic shape easily seen in the bathymetry (dot line in Fig. 3). Amplitude wipeout is present beneath bright areas as well as overlying anomalies in the free-gas trapping layer in the same time range to Line37ns (box 2a and 2b, Fig. 15).

6.3. Line20ew

Line20ew, as seen in Fig. 3, runs across the northern limits of the mound and intersects the lines 17 and 37. This line offers clues relating to all of the aforementioned lines. The, amplitude brightening is well imaged as a funnel shape anomaly, which originated at about 1.4 s, seems fill the mini basin present in the shallow section (Fig. 16, box 1). This mini basin .is the same imaged in line 17, and appears to be formed by the movement of the large normal fault on the east. . This fault is the relevant structural feature reaching the deepest high amplitude phase reversal bright spot (Fig. 16 box 2b). The negative polarity bright spot continues, as segmented and discontinuous horizons moving westward and, box 2a in Fig. 16 shows the detail of such horizon. Across the section wipeout zone in chimney like structures are present and generally overlay the reverse polarity bright spot.

6.4. High-resolution interpretability

The shallow, filled basin in Line17ns and Line20we overlies a large growth fault and contains a high degree of amplitude variation. This is the new form of high-frequency brightening and indicates that the employed processing technique complements the high sampling frequency. The box 1 in Fig. 16 shows the close-up of the basin. A conservative velocity estimate of 1600 m/s for unconsolidated sediments in the basin suggests the maximum depth below the seafloor in Fig. 17 is approximately 50 m. The lateral extent of this view is roughly 1 km. Temporal resolution of geologic information in this view is on the order of microseconds which converts to centimeter resolution. Phase of the signal at this resolution is maintained across the entire kilometer wide basin. Clear evidence is presented showing that the amplitude brightening effect in the shallow sediments results from the presence of a high-frequency sedimentary response and exists on very small spatial scales. This phenomenon appears to be a higher order process acting within the strata. Both two consortium cruises in April 2008 and June 2011 successfully retrieved cores containing significant solid hydrates in form of chunks and nodules from sediments showing the high-frequency brightening characteristics, an example of core inclusions is shown in Fig. 17, the sample comes from a gravity core collected over an area where the high frequency scatter were identified in the seismic record (see Fig. 3 for core location). We speculate that hydrocarbon fluids moving along the fault, which works as preferred conduit for fluid migration, entering in the shallow sediments layers, might freeze forming gas hydrates. The solid hydrates behave as solid inclusions imbedded in a homogeneous media, and, therefore, scattering back the seismic energy and producing the brightening effects in the seismic record. Further research is underway to continue ground-truthing this occurrence, and physically explain how the two phenomena are related.

7. Conclusions

The benefits of using EMD with seismic reflection data have been noted by Magrin-chagnolleau and Baraniuk (1999) and Battista et al. (2007). However, the EMD is adapted here to allow for far more flexibility separating signal from noise and doing so with significantly increased computational efficiency. Further, band modulating the EMD by mode weighting proves to be a powerful tool in manipulating

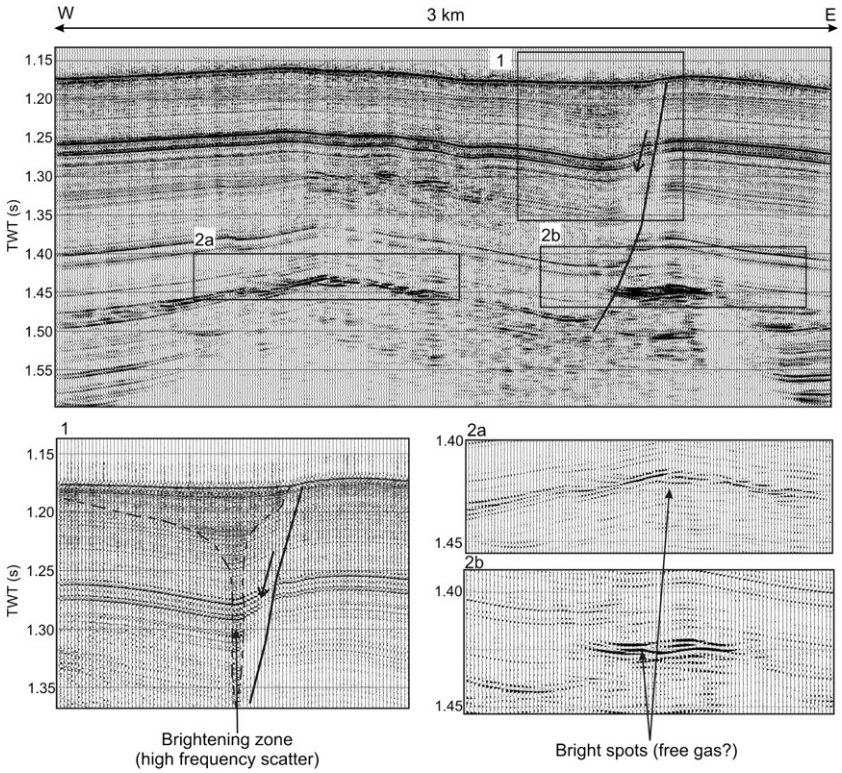

Fig. 16. Processed Line20ew. Line20we runs east (right) to west (left). No seafloor venting is observed even though there appear to be several signs of migration pathways. The box 1 highlights the amplitude brightening associated with the filled basin in the shallow sediments. The anomaly has a characteristic funnel shape, as described in the zoomed picture. A prominent normal fault generates the growing basin and probably is the conduit where hydrocarbon fluids pass. Free gas may be trapped below the reverse polarity bright spot highlighted in box 2a and 2b.

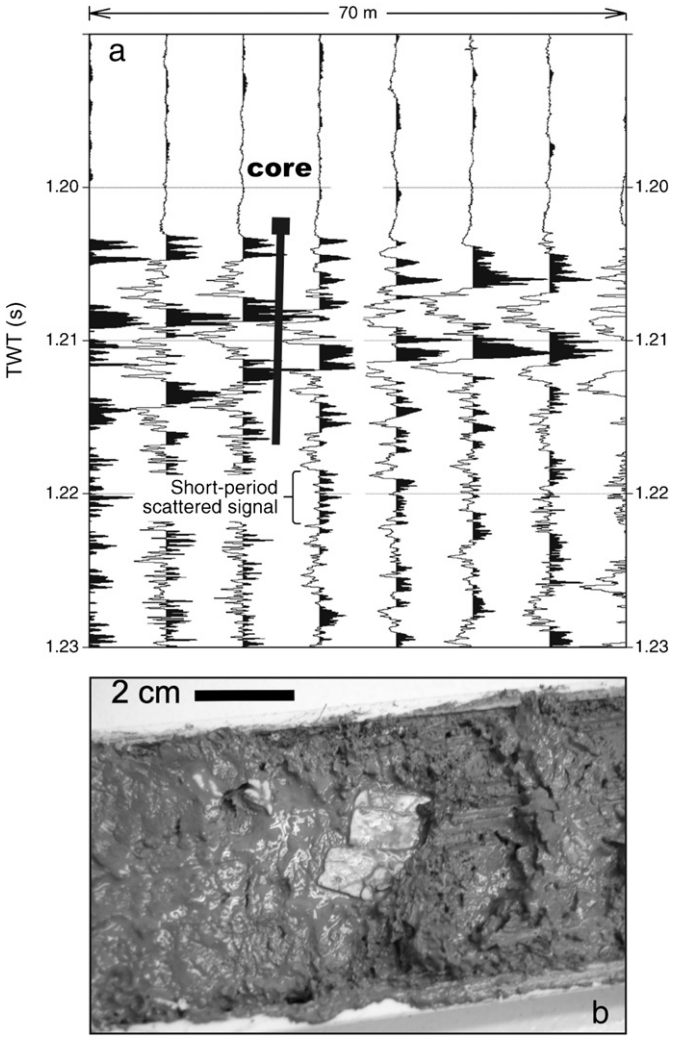

Fig. 17. Amplitude brightening anomaly ground truthing. The new brightening amplitude mapped in the seismic data and interpreted as high frequency scatter (a) has been ground truthing via gravity core. Core, (position in Fig. 3) has recovered inclusions of solid hydrates within the sediment (b). We speculate that the seismic anomaly is generated by the presence of solid hydrates in the sediment that scatter the seismic energy. Only high resolution processing is able to image such phenomenon.

seismic reflection data without damaging phase and amplitude. The weighted-mode empirical mode decomposition has demonstrated its ability to optimally suppress noise and enhance geologic information in seismic reflection data. All of the structures outlined by Hardage and Roberts (2006) are imaged with high quality and therefore, the technique may be considered as a significant advancement in "seismic technology" It has also proven itself to be an extremely diverse utility for use with high-resolution seismic reflection data and in imaging structures related to hydrate systems. A new and poorly understood very-high frequency brightening effect in the shallow sediments is successfully imaged and well suited for quantitative analysis using (un)conventional techniques. Therefore, the future direction of the weighted-mode EMD is to afford additional processing of the highest quality data for characterizing the new trends imaged with high-resolution seismic profiling.

Acknowledgments

This paper is dedicated to the memory of Dr. J. Robert (Bob) Woolsey Jr., long-time Director of MMRI-CMRET at The University of Mississippi and founder/Director of the GOMHRC. Bob was an outstanding scientist, an incredible man and colleague, and incomparable friend.

Authors are grateful to: Tom McGee at MMRI and Vaughn Goebel of Lookout Geophysics; to MMRI-CMRET-STRC Research Systems Specialists Brian Noakes, Andy Gossett and Matt Lowe and Electronics Technician, Larry Overstreet, to the Louisiana Marine Consortium (LUMCON) and the Captain and Crew of the R/V Pelican for at-sea support.

This project has been supported by Gulf of Mexico Hydrates Research Consortium through funds provided by DOI BOEMRE, DOE National Energy Technology Laboratory, and DOC-NOAA's National Institute for Undersea Science and Technology (NIUST).

References

Addison, A.D., Battista, M.B., Knapp, C.C., 2009. Improved hydrogeophysical parameter estimation from empirical mode decomposition processed ground penetrating radar data. Journal of Environmental and Engineering Geophysics 14, 171–178.

Battista, B.M., Knapp, C.C., McGee, T.M., Goebel, V., 2007. Application of the empirical mode decomposition and Hilbert-Huang transform to seismic reflection data. Geophysics 72, 29–37.

Battista, B.M., Addison, A.D., Knapp, C.C., 2009. Empirical mode decomposition operator for dewowing GPR data. Journal of Environmental and Engineering Geophysics 14, 163–169.

Hardage, B.A., Roberts, H.H., 2006. Gas hydrate in the Gulf of Mexico: what and where is the seismic target? The Leading Edge 25, 566–571.

Huang, N., Shen, Z., Long, S., Wu, M., Shih, E., Zheng, Q., Tung, C., Liu, H., 1998. The empirical mode decomposition method and the Hilbert spectrum for non-stationary time series analysis. Proceedings of the Royal Society London A454, 903–995.

Knapp, J.H., Knapp, C.C., Macelloni, L., Simonetti, A., Lutken, C.B., 2010. Subsurface Structure and Stratigraphy of a Transient, Fault-Controlled Thermogenic Hydrate System at MC-118. Gulf of Mexico AAPG Annual Meeting Trans., New Orleans (LA) April 11- April 14 2010.

Lapham, L.L., 2008. Towards the development of a biogeochemical model to describe venting activity at MC 118. Proceedings of the Gulf of Mexico Hydrates Research Consortium, Semiannual Meeting. Oxford MS, Feb. 26–27, 2008.

Lapham, L.L., Chanton, J., Martens, C., Sleeper, K., Woolsey, R.J., 2008. Microbial activity in surficial sediments overlying acoustic wipeout zones at a Gulf of Mexico cold seep. G^3. 9, 17.

Lutken, C.B., Lowrie, A., Geresi, E., Bennett, R., Faas, R., Battista, B.M., McGee, T.M., 2003. Interpretation of high resolution seismic data from a geologically complex continental margin, northern Gulf of Mexico. GCAGS/GCSSEPM Transaction 53, 504–516.

Macelloni L., 2005. High-resolution marine digital seismic method: theoretical constrains, digital processing, new developments. PhD Dissertation, "La Sapienza" University of Rome. Pages 171. PADIS - Pubblicazioni Aperte Digitali Interateneo Sapienza [PHD–2005-187] http://hdl.handle.net/10805/812

Macelloni, L., Caruso, S., Lapham, L.L., Lutken, C.B., Brunner, C., Lowrie, A., 2010. Seafloor bio-geological and geochemical processes spatial distribution as proxy to evaluate fluid-flux regime and time evolution of a complex carbonate/hydrates mound, northern Gulf of Mexico. 2010 GCAGS/GCSSEPM Trans.

Magrin-chagnolleau, I., Baraniuk, R.G., 1999. Empirical mode decomposition based time-frequency attributes. Proc. 69th SEG Meeting.

McGee, T.M., 1997. High-resolution seismic in the frequency domain: an illustrated overview. European Journal of Environmental and Engineering Geophysics 2, 205–222.

McGee, T.M., 2000. Pushing the limits of high-resolution in marine seismic profiling. Journal of Environmental and Engineering Geophysics 5, 43–53.

McGee, T.M., 2006. A seafloor observatory to monitor gas hydrates in the Gulf of Mexico. The Leading Edge. 25, 644–647.

Pai, F.P., Huang, L., Hu, J., Langewish, D.R., 2007. Time-frequency method for nonlinear system identification and damage detection. Structure Health Monitor 7 (2), 103–125.

Rilling, G., Flandrin, P., Goncalves, P., 2004. Detrending and denoising with empirical mode decomposition. 12th European Signal Processing Conference.

Sassen, R., Roberts, H.H., Jung, W., Lutken, C.B., DeFreitas, D.A., Sweet, S.T., Guinasso Jr., N.L., 2006. The Mississippi canyon 118 gas hydrate site: a complex natural system. OTC Paper #18132; Offshore Technology Conference, Houston, TX.

Schmitt, F.G., Huang, Y., Lu, Z., Brizard, S., Molinero, J.C., Liu, Y., 2007. Analysis of nonlinear biophysical time series in aquatic environments: scaling properties, and empirical mode decomposition. Nonlinear Dynamics in Geosciences, pp. 261–280.

Sleeper, K., Lowrie, A., Bosman, A., Macelloni, L., Swann, C.T., 2006. Bathymetric mapping and high resolution seismic profiling by AUV in MC 118 (Gulf of Mexico). OTC Paper # 18133, Offshore Technology Conference, Houston, TX.

Sweeney-Reed, C.M., Nasuto, S.J., 2007. A novel approach to the detection of synchronization in EEG based on empirical mode decomposition. Journal of Computational Neuroscience 23, 79–111.

Wood, W., Gettrust, J., Chapman, R.N., Spence, J., Hyndman, R., 2002. Decreased stability of methane hydrates in marine sediments owing to phase-boundary roughness. Nature 420, 656–660.

Wood, W., Hart, Patrick E., Hutchinson, Deborah R., Dutta, Nader, Snyder, Fred, Coffin, Richard B., Gettrust, Joseph F., 2008. Gas and gas hydrate distribution around sea floor seeps in Mississippi Canyon, northern Gulf of Mexico, using multi-resolution seismic imagery. Marine and Petroleum Geology 25 (9), 952–959 November 2008.

Wu, Z., Huang, H., 2004. A study of the characteristics of white noise using the empirical mode decomposition method. Proceedings of the Royal Society London 460, 1597–1611.

Wu, Z., Huang, N.E., Long, S.R., Peng, C.-K., 2007. On the trend, detrending and variability of non-linear and non-stationary time series. Proceedings of the National Academy of Sciences of the United States of America 104 (38), 14889–14894.

Ziolkowski, A., Parkes, G., Hatton, L., Haugland, T., 1982. The signature of an air gun: computation from near field measurements. Geophysics 47, 1413–1421.

Ziolkwoski, A., 1987. The determination of the far-filed signature of interacting array of marine seismic sources from near-field measurements. Result from delft air gun experiment. First Break 5 (1), 15–29.